

Egyptian Journal of Geology

https://egjg.journals.ekb.eg



Remote Sensing and Geophysical Studies to Delineate Gological and Tectonic Elements of The East Uweinat\Gilf Kebir Basin Area, Southwest Western Desert, Egypt



Ahmed A. Elhusseiny $^{(1)}$, Tamer Farag $^{(1)}$, Khalid Khalifa $^{(2)}$, Shaimaa Abd El Raheem $^{(2)}$ and Alaa Aref $^{(1)}$

THE BASIN of Gilf Kebir is located in the southwest region of the Western Desert of Egypt. The lithologies and geological structures in the area indicates that it has the perfect formation system of Paleozoic intra-cratonic rift. This study analysed and integrated the interpretation of remote sensing (Landsat 9), geophysical (aeromagnetic and satellite gravity data), and geological data to understand the underlying structure of the area of Gilf Kebir Basin. Basins of the Paleozoic intracratonic formed within the African Shield subsequent to the deformation and plutonism of Precambrian. A thick clastic Gilf sandstone was deposited between the two major plutons of the Uweinat area in the west and the Tarfawi area in the east. The dominant structural tendencies are NE-SW/ENE-WSW, E-W, and NW-SE/NNW-SSE. The depths in the basin were determined using a three-dimensional (3D) depth inversion. The results show that the thickness of the sedimentary section ranges from zero (basement outcrop) to more than 3000 meters. Remote sensing data clarify that there are some alteration processes that some of the rocks in the area have been exposed to, which are consistent with the geological map. In addition, the locations of Fe-silicate mineralization are consistent with the basement rocks shown in the geological map. By integrating magnetic and satellite gravity data, we conclude that in the Gilf Kebir area, there are good conditions of hydrocarbon source-reservoir-cap assemblage.

Keywords: Magnetic Interpretation, East Uweinat, Gilf Kebir Basin, Tectonic Elements, Remote sensing data.

1. Introduction

This study analyzes and interprets aerial magnetic data from the East Uweinat/Gilf Kebir region in Egypt's Southwest Western Desert, integrated with remote sensing data analysis. Figure 1-a illustrates the geographical extent of the study area. Beyond contributing to a broader comprehension of the regional tectonic framework and structural evolution, the primary aim of this research is to deliver comprehensive structural characterization within the East Uweinat/Gilf Kebir exploration area. This information is intended to augment forthcoming seismic investigations, particularly in sectors where seismic coverage is limited or where intraformational lithological variations fall below the resolution threshold of seismic techniques. Based on the scope of work, the ultimate objectives of this study are as following:

- Mapping geological trends.
- Mapping mineralization zones.
- Mapping the boundary of the basin.
- Estimating the depths to magnetic sources.

 Inferring the groundwater/hydrocarbon potentials of Gilf Basin.

The interpretation did show that the fields in question could possibly be extended and drill sites could be added. Integrated interpretation of the magnetic data, in accordance with the available remote sensing and geological information, enabled more precise delineating of the detailed structural configuration of surface and the buried subsurface basement complex.

2. Tectonic history of the east Uweinat\Gilf Kebir Area

From a tectonic perspective, it is widely accepted that Egypt can be subdivided into six distinct tectonic domains (Figure 1-b; Meshref, 1990), each exhibiting unique structural characteristics and geological evolution. These tectonic provinces include: (1) the Arabian-Nubian Shield, (2) the Stable Shelf, (3) the Unstable Shelf, (4) the Red Sea and Gulf of Suez Rift, (5) the Gulf of Aqaba, and (6) the Delta Hinge Zone.

⁽¹⁾ Nuclear Materials Authority (NMA), Egypt

⁽²⁾ South Valley Egyptian Petroleum Holding Company (Ganope), Egypt

2.1. The Arabian-Nubian Shield (ANS)

The Precambrian crystalline basement underlying Egypt and Sudan, referred to as the Arabian-Nubian Shield (ANS), stretches from the Nile River eastward toward the Arabian Peninsula (see Figure 1-b). Southward, the ANS is contiguous with the Mozambique Belt. Geologically, the ANS is widely understood to have formed during Neoproterozoic through the complicated accretion of various terranes atop an older pre-Pan-African basement, commonly designated as the Nile or East Sahara craton (Dixon and Golombek, 1988; Vervoort and Blichert-Toft, 1999; Ren and Abdelsalam, 2006).

The initial stage in the evolution of the ANS involved the accretion of numerous terranes and volcanic arcs, predominantly comprising complex sequences of mafic (basaltic-andesitic) to felsic (rhyolitic-dacitic) volcanic and sedimentary assemblages (Kroner et al., 1987; Harris et al., 1993; Stein and Goldstein, 1996).

This shield encompasses Precambrian lithologies from the Southwestern Desert, including the Uweinat Mountain region. The ANS is characterized by intensely deformed igneous and metamorphic units, exhibiting prominent folding, thrusting, shearing, extensional fracturing, and the intrusion of dykes. Major structural lineaments within these rocks trend predominantly north-south and east-west (Stern, 1994; Abdelsalam and Stern, 1996; Ren and Abdelsalam, 2006). After a prolonged interval of erosion, these basement rocks were largely overlain by sand deposits during the Cretaceous (circa 90 million years ago), giving rise to the Nubian Sandstones. Subsequent continental uplift associated with the Red Sea rift system led to the erosion of these sandstones along the rift margins.

2.2. The stable shelf

Stable shelf constitutes the southern and middle portions of both Eastern and Western Desserts as well as mid Sinai. It is characterized by (Meshref, 1990):

- 1. Thin sedimentary cover, ranging, in thickness, from ~400 m in south to 1000 m in north and, in age, from Paleozoic to Middle Eocene. However, isolated basins containing a thick pile of sediments reaching to 4000 m are recently recorded; firstly, via aeromagnetic survey and later documented by drilling (e.g., Kom Ombo basin and Kharit basin at the southern Nile Valley and Eastern Desert).
- 2. Structurally, this shelf is less deformed than the unstable shelf. It is mainly affected by faulting with minor role of folding.

2.3. Geological and structural setting

Paleozoic intra-cratonic basins emerged within the African Shield subsequent to Precambrian tectonic reworking and magmatic activity. Notably, two principal plutonic bodies have been delineated: one situated in the western Uweinat region and another in the eastern Tarfawi locality. Between them, a thick clastic section of the Gilf Sandstone was deposited (Figure 1-c, Conoco and EGPC, 1987). The Lower Paleozoic rocks are almost absent in the West, while slightly folded Devonian-Carboniferous sediments are well developed.

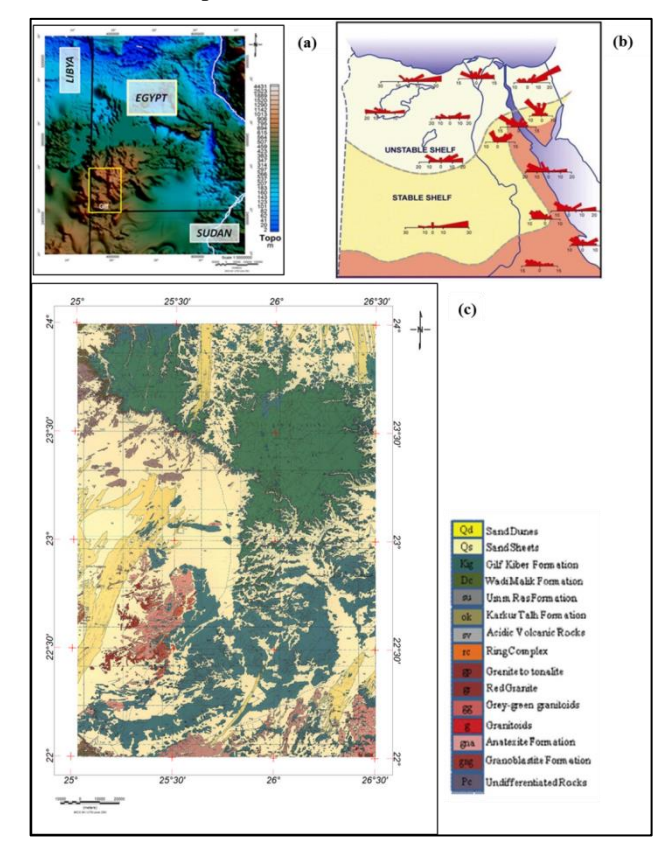


Fig. 1. (a) Location map of East Uweinat/Gilf Kebir area. (b) Major tectonic unites and trends in Egypt (after Meshref, 1990). (c) Geologic Map (after Conoco and EGPC, 1987).

The Landsat image of East Uweinat/Gilf Kebir area (Figure 2) shows that the main structures trends are as following:

- NNE-SSW trending Gilf Faults
- NW-SE trending Kamel Faults
- Several East-West faults have been identified.

These trends are normal gravity faults. The configuration and sediments distribution of the NNE-SSW Gilf trending suggests that the NE-SW trending Uweinat Basement Block was developed by post-Carboniferous orogenic movements and the Tarfawi Basement Block was uplifted at the end of the Paleozoic. Cretaceous and younger sediments lie on the Tarfawi High, while only Cretaceous-Oligocene igneous rocks are observed on the Uweinat High.

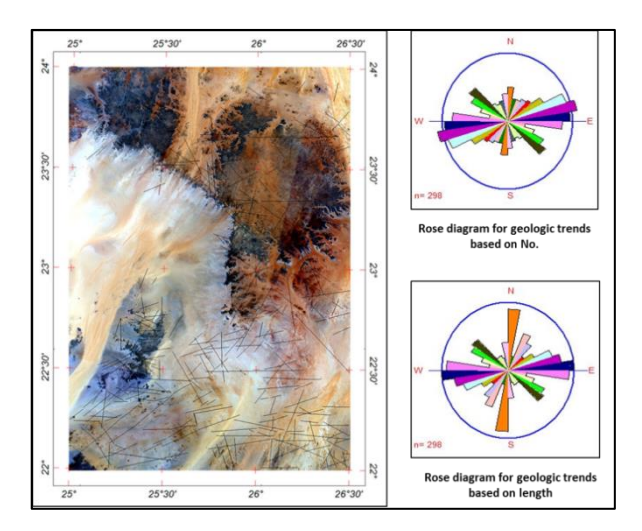


Fig. 2. Radiometrically corrected Landsat ETM+ Mosaic of East Uweinat/Gilf Kebir area, southwestern Egypt with surface lineaments and structural trend analysis.

3. Geophysical And Remote Sensing Data

In 2011, the Airborne Geophysical Department, Nuclear Materials Authority conducted an Airborne geophysical survey at the East Uweinat\Gilf Kebir area on behalf of Ganoub El Wadi Holding Petroleum Company (Ganope) as a part of the program of the petroleum assessment. The data were acquired along flight lines in the direction of N-S with 2.0 kilometer spacing, while the tie lines spacing was 10 kilometers and the direction was E-W. The flight altitude was at 100 m ground clearance (NMA, 2011).

The satellite gravity data is derived from the Altimetric Marine Gravity Field (Anderson, 2013). Satellite altimetry is a very important source of information for the determination of the figure and gravity field of the Earth. The height of the oceans closely assembles an equi-potential surface of gravity and can be used to define the high-resolution marine gravity field.

Remote sensing offers valuable insights into the chemical composition of rocks and minerals on Earth's surface, particularly in areas that are not totally covered by vegetation or sand dunes. Five cloud-free Landsat 9 scenes were downloaded from the United States Geological Survey (USGS) Earth explorer website and have been already georeferenced to the UTM zone 35N using the WGS-84 datum. The acquisition period was August 2023, corresponding summer season. The Landsat 9 data have been subjected to several processing using In Environment for Visualizing Images (ENVI) software.

4. Geological Mapping From Potential Field Data

The primary objective of image enhancement in the analysis of potential field data is to suppress irrelevant components of the gravitational or magnetic signals, thereby accentuating anomalies that correspond to subsurface geological structures relevant to the investigation. In the context of basin analysis, the focus is on amplifying signals associated with sedimentary bodies and structural features within and beneath the basin framework. This typically entails isolating the long-wavelength components related to deeper crustal structures.

Standard techniques employed include frequency filtering, calculation of gradients, and the subtraction of regional fields modeled via polynomial surface fitting. Additional approaches exist to delineate the probable geometry of source bodies responsible for gravity and magnetic anomalies, as well as to automate the detection of linear features indicative of faults and basement structural trends.

4.1Magnetic Source Bodies for Geological Mapping

The spatial localization of geological source bodies can be refined through the combined analysis of vertical and horizontal gradients of the magnetic field, which manifest as magnetic anomalies. The analytic signal (AS), defined as the square root of the sum of the squares of the vertical and horizontal derivatives of the magnetic or gravitational field, provides a composite gradient measure (Roest et al., 1992). The position of the causative bodies governs the shape of the AS and is independent of the magnetization vector orientation. This property renders the analytic signal particularly effective in identifying remanent magnetization, which is a magnetic signature retained from past geological processes rather than induced by the present geomagnetic field.

The amplitude of the analytic signal facilitates geological interpretation by being strictly positive, with maxima located directly above magnetic sources or their boundaries (MacLeod et al., 1994; Li, 2006; Li et al., 2008). AS analysis effectively reduces magnetic data to anomalies whose peaks correspond to edges or centers of magnetized bodies, enabling depth estimation of these sources.

The utility of the AS method has been demonstrated in mapping magmatic bodies within the East Uweinat/Gilf Kebir Basin. The AS map (Figure 3-b) reveals sharper contrasts between tectonic units (Figure 3-c) than those detectable from total magnetic field anomalies alone (Figure 3-a). A pronounced boundary delineated by the AS corresponds to magnetic sources separating the East Uweinat Mountain from the Gilf Kebir Basin. High AS amplitude zones dominate the northwestern, central, and southern sectors, coinciding with the East Uweinat Mountain and extending southeastward. Conversely, magnetically subdued regions in the northern and eastern parts align with sub-basinal areas characterized by thick sedimentary sequences exhibiting low magnetic susceptibility, such as those in the Gilf Basin. Linear high AS features along the northern, southern, and eastern margins correspond to inferred near-surface dykes and volcanic ridges (Figure 3-b).

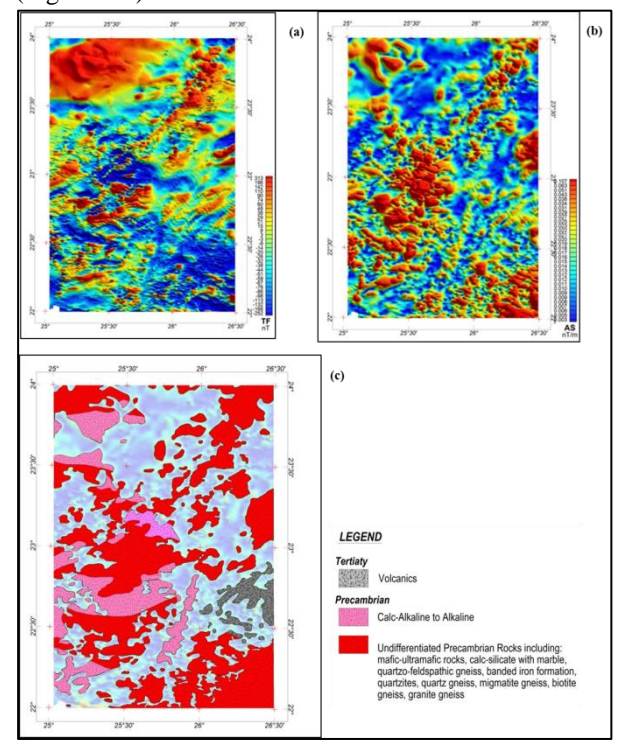


Fig. 3. Maps showing magnetic data used to infer basement composition. (a) Total intensity magnetic field (TF) of the East Uweinat/Gilf Kebir area, southwestern corner of Egypt (after NMA, 2011). (b) Analytic Signal (AS). (c) Near-Surface magnetic source boundaries.

Following the computation of the analytic signal, polygons can be delineated around positive AS peaks to approximate the geometry and boundaries of independent magnetic source bodies, magnetization direction. This facilitates an objective extraction of geological information geophysical datasets (Gibson et al., 2011; Morse, 2010). Figure 3-c presents such polygons outlining magnetic sources within the East Uweinat/Gilf Kebir Basin, derived from the AS map (Figure 3-b), itself calculated from total magnetic intensity data (Figure

3-a). To mitigate noise effects, upward continuation to 1000 meters was applied before AS calculation.

By correlating these magnetic source polygons with basement lithologies exposed at the surface (Figure 3c), the spatial distribution of discrete near-surface basement domains can be inferred in areas lacking direct geological data. The figure demonstrates that regions where the basement comprises less magnetic metasedimentary or granitic units (depicted in magenta) and more magnetic meta-igneous units (shown in red) are encompassed within distinct magnetic source polygons. Additionally, intra-basinal volcanic activity is documented in the southern subbasins. This spatial association between basement lithology and magnetic source polygons suggests that magnetic anomalies in this region predominantly reflect variations in magnetized basement rock presence (Hall et al., 2012).

Partitioning the basement into discrete domains bears implications for hydrocarbon prospectivity, as variations in basement composition can influence heat flow regimes. These variations affect the thermal maturation of overlying sedimentary sequences and consequently the generation potential of source rocks. Nonetheless, interpretations of basement domains based on source polygons constitute preliminary approximations of magnetic source distribution within the basement or sedimentary cover. Therefore, after mapping and geological calibration of these polygons, their validity should be further assessed through detailed forward and inverse modeling.

4.1. Mapping Geological Trends

Analyzing structural trends within sedimentary basins is critical for delineating basement zones distinguished by unique structural fabrics and for evaluating basement influences on basin evolution. Multiple automated methodologies exist for extracting directional trends from gravity and magnetic datasets. These techniques capitalize on the observation that significant gradients in gravity and magnetic measurements frequently result from the juxtaposition of lithologically distinct materials exhibiting variable physical properties, such as density and magnetic susceptibility, across subsurface boundaries.

Consequently, the Total Horizontal Gradient (THG; Figure 4-b), Second Vertical Derivative (SVD; Figure 4-c), and Tilt Derivative (Figure 4-d) were computed from the Reduced to the Pole (RTP; Figure 4-a) magnetic anomaly data, which represent rates of change or gradient magnitudes in the magnetic field (Cordell and Grauch, 1985; Blackely and Simpson, 1986; Salem et al., 2008). These derivatives facilitated the identification of principal magnetic lineaments (see Figure 5).

Interpretation of the magnetic anomaly maps for the East Uweinat/Gilf Kebir Basin reveals a geologically complex region dominated by extensive magnetic lineaments oriented NW-SE, NNE-SSW, sub-E-W, and sub-N-S (Figure 5). The spatial distribution of magnetic anomalies (Figure 5) supports the subdivision of this region into discrete domains characterized by distinctive anomaly patterns. The Gilf Kebir (GK) sector, for instance, is defined by prominent NNE-SSW oriented anomalies (the Dakhla Structural Trend), displaying high-frequency, highamplitude magnetic signatures (Figure 4), which contrast with adjacent zones exhibiting loweramplitude, intermediate-to-low anomaly values and comparatively subdued magnetic fields (Figure 4-a). Broad, long-wavelength negative anomalies identified in the northern and eastern portions of the study area are inferred to be related to deeper crustal structures and thick accumulations of sedimentary cover. The southeastern domain (East East Uweinat – EEU) area is characterized by the presence of near-surface volcanic intrusions. The East Uweinat domain (EU) shows a ring complex-like pattern with structural trends of E-W. N-S and NE-SW.

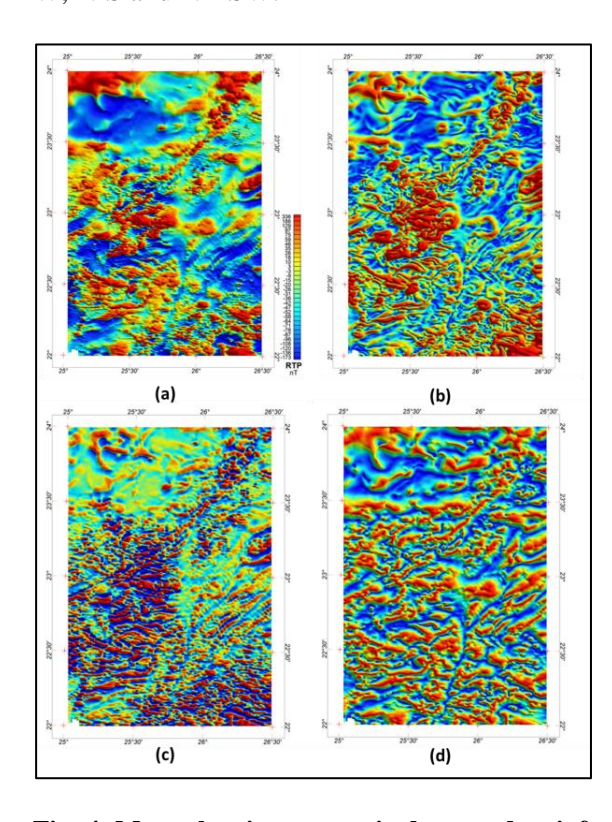


Fig. 4. Maps showing magnetic data used to infer basement geological trends. (a) Reduced to Pole magnetic data (RTP). (b) Total horizontal derivative (HG). (c) Second vertical derivative (SVD). (d) Tilt derivative. b, c and d after RTP upward continued to 1.0km.

Satellite altimetric measurements have facilitated the widespread acquisition of global geoid and gravity data, particularly in remote regions. Although individual satellite altimetry observations may not match the precision of direct marine gravity measurements, their capacity to deliver consistently reliable gravity data on a near-global scale renders satellite altimetry indispensable and superior for the determination of the Earth's global marine gravity field. ocean surface slope is related to the geoid, the equipotential surface that best fits mean sea level. Gravity anomalies can be computed from the derivative of potential, so ocean surface slope measurements can be used to infer gravity anomalies for the world (Anderson, 2013).

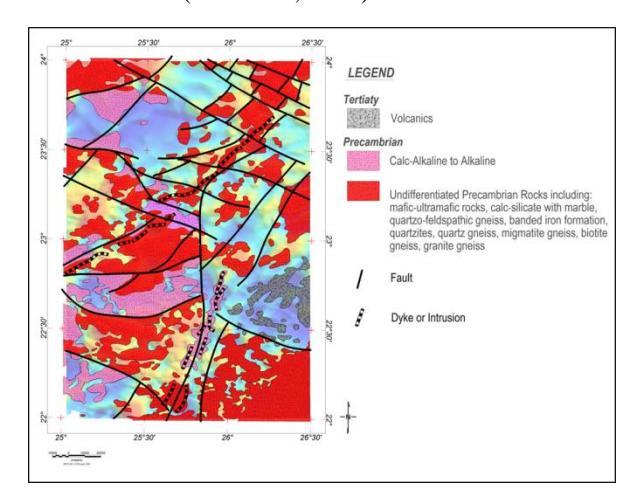


Fig. 5. Map showing basement composition and major trends derived from the magnetic data overlain on the reduced to the pole magnetic data.

The Bouguer gravity anomaly for the East Uweinat/Gilf Kebir region (Figure 6-a), calculated utilizing satellite-derived gravity measurements and adopting a mean density of 2.3 g/cm³, exhibits a persistent long-wavelength component. This feature reflects changes in crustal thickness throughout the area, characterized by high values over oceanic domains, relatively low values over continental regions, and a pronounced gradient demarcating their boundary. Eliminating the long-wavelength field as a "regional" field from the Bouguer gravity field will enhance the information on crustal structure.

Depth slicing is utilized to separate distinct wavelength components of the bouguer data set using spectral analysis (Spector, 1968). Pseudo-depth slicing improves the impacts of sources at any selected depth while reducing the effects of deeper or shallower sources.

In the filtration process, filtration operation has a great important role in the different interpretation tools. So, the high-pass filtering tool (e.g., Butterworth filtering technique or the orthogonal polynomial tool) is achieved. For gravity data, three segments chosen also to represent average pseudo-

depths of, which could be equivalent to different wavelengths of < 500 km "deep high-pass (Figure 6-b), < 250 km "intermediate high-pass (Figure 6-c) and < 52 km relatively shallow high-pass (Figure 6-d), respectively.

Identification of edges and structural boundaries derived from gravity data (Figure 6-d) and magnetic anomalies (Figure 5) emphasizes the role of the basement in controlling the fault configuration within the superimposed sedimentary basin. The observation that fault orientations inferred from gravity data closely align with the structural grain delineated by magnetic data implies that reactivation of basement faults has played a significant role in shaping both basin development and its structural deformation styles. This correspondence underscores the pronounced control exerted by the basement architecture on fault propagation and distribution in the overlying sedimentary sequences.

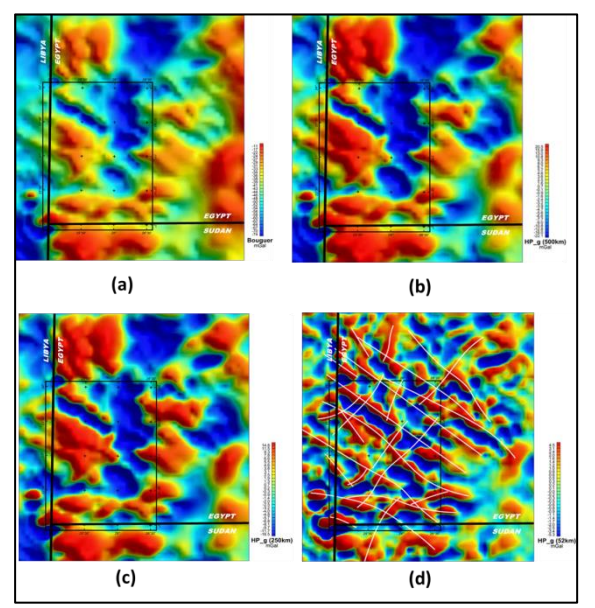


Fig. 6. Maps showing satellite gravity data used to infer basement geological trends in East Uweinat/Gilf Kebir area and its vicinity. (a) Bouguer gravity anomaly data. (b) High-pass gravity component at wavelength 500 km. (c) High-pass gravity component at wavelength 250 km. (d) High-pass gravity component at wavelength 52 km overlaid by structure lineaments inferred from gravity data. Box in black is the study area

4.2. Estimating Depth to Basement

There is no available information on subsurface basements in the East Uweinat/Gilf Kebir basin. For example, there are no wells or seismic traverses to constrain magnetic basement depth estimates. The primary exploration challenges in this region are the complex basement faulting and structural system. The complex basement structure results from the varying ages of faults and the difficulties in defining the time sequence.

Three-dimensional (3D) forward modeling and inversion of potential field data were applied to the East Uweinat/Gilf Kebir region. The main aim was to characterize the subsurface basement topography utilizing Oldenburg's spectral layered-earth inversion approach (Oldenburg, 1974). It is important to emphasize that the depth estimates for the basement obtained through this method may not precisely correspond to the actual basement depths. Based on our experience in interpreting potential field data, these depth estimates generally approximate the true values; however, they tend to be somewhat overestimated. This challenge in interpretation can be mitigated by inverting the magnetic data, which enables a more accurate assessment of basement structure. In this context, inversion refers to an automated computational technique that generates a geological subsurface model by integrating observed magnetic data with a priori geological information. The resulting three-dimensional representation of the basement is illustrated in Figure 7.

The area is characterized by an uplifted basement in the central and southern parts related to the basement complex of East Uweinat mountainous area. It is directed in the general NE-SW direction (Trans African trend) with exposed basement to west and south. The depth values are getting deeper to the north and to the east.

The area also is characterized by the presence of two major sub-basins; one of them is located in the northwestern part of the area and the other is located in the southeastern part. The depth values get deeper in the center of the northern basin reaching a value of 3500 m. The depth to the basement values gets shallower in the southern basin reaching a value of 2500 m. It is clear from depth to basement map that this basin is going to be more deeper to the east, outside the limits of the area under study. It is also observed that the main basins are dissected by several faults forming relatively small sub-basins.

5. Alteration Zones

Remote sensing techniques play a crucial role in identify lithological lithologies related to geological structures, including their potential subsurface continuities (Ramsay and Huber, 1987). Various methodologies, such as spectral band ratio analysis and principal component analysis (PCA), can effectively delineate hydrothermal alteration zones prospective mineralized regions within multispectral datasets, such as those derived from Landsat data (Sabins, 1997; Goetz et al., 1983; Rowan et al., 1986; Abrams and Hook, 1985; Okada et al., 1993; Amuda et al., 2014; Poormirzaee and Oskouei, 2010; Ramadan et al., 2001; Mia and Fujimitsu, 2012). Specifically, the application of band ratios to multispectral data has proven successful in detecting zones of hydrothermal alteration (Sabins, 1999; Mia and Fujimitsu, 2012; Aydal et al., 2007; Liu et al., 2013; Tangestani and Moore, 2000), which are often linked to mining activities and can cause significant modifications to the mineralogical properties of local lithologies.

For this study, bands 2 through 7 were mosaicked and subsetted to focus on the target area. Red, green, and blue (RGB) band combinations, alongside computed band ratios, were employed on the Landsat dataset to facilitate the discrimination of diverse lithologies and iron-rich rocks. Variations in color within these combinations are indicative of differences in rock origin and mineral assemblage. Numerous researchers have leveraged band ratios to accentuate particular spectral features by dividing the digital number (DN) values between specific bands, thereby enhancing geological interpretation (Gabr et al., 2010; Pour and Hashim, 2011; Amer et al., 2012; Pour et al., 2019c; Sekandari et al., 2020a; Ishagh et al., 2021).

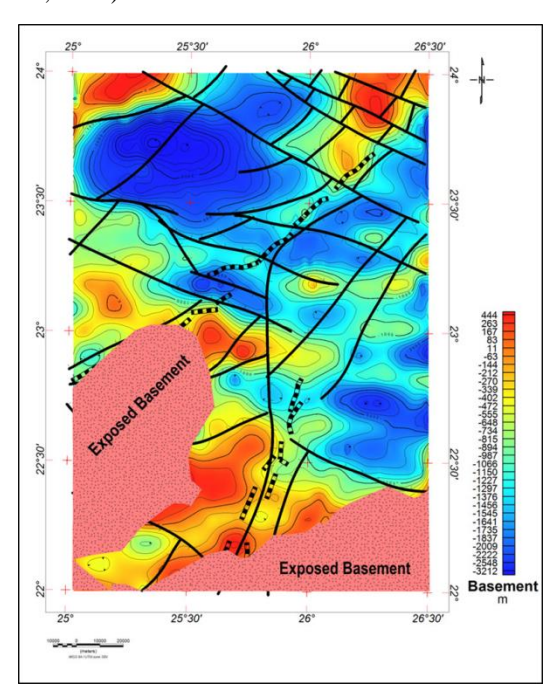


Fig.7. Depth to magnetic basement overlaid by major magnetic trends.

Using combination of bands (4, 3, and 2) in RGB to discriminate the different rock units in the area in true color (Figure 8). The map distinguishes the different rock units in the area similar to the lithological map of CONCO map. The basement rock appears in dark colors while sedimentary rocks appear in light colors. The sand sheets and dunes cover most of the area. The sand dunes extend and spread in NE - SW direction, which is the same direction as the extension of the basement rocks.

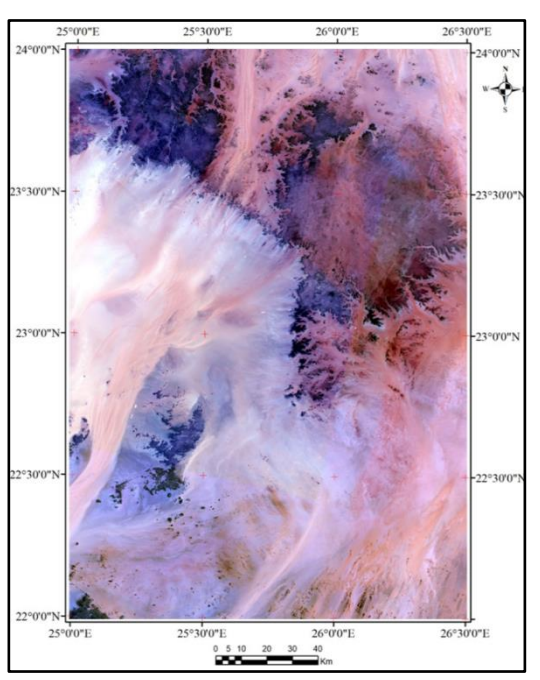


Fig. 8. Band combination of bands (4, 3, and 2) in RGB respectively.

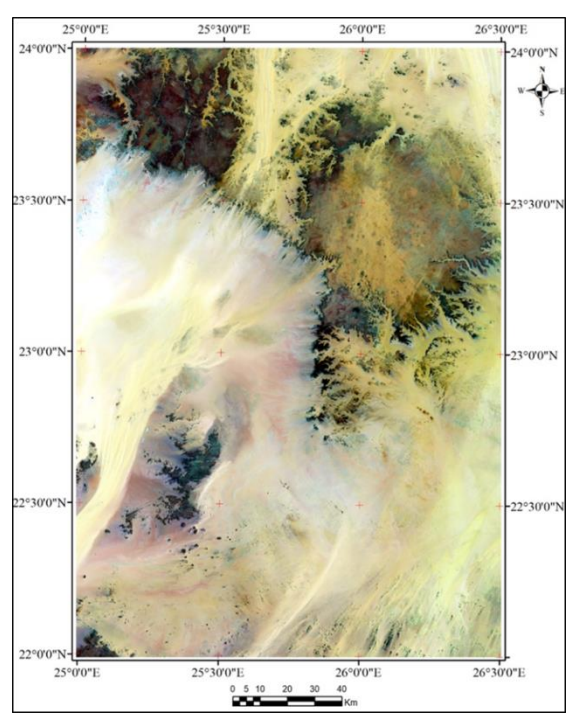


Fig. 9. Band combination of bands (7, 5, and3) in RGB respectively.

Conversely, an RGB composite utilizing bands 7, 5, and 3 has been employed to distinguish various lithological units in false color imagery (see Figure 9). Within this combination, felsic rocks are represented by a reddish-brown hue, mafic rocks are displayed as dark tones, and wadi deposits are characterized by their high brightness.

Band ratio techniques are extensively adopted in mineral exploration to enhance the spectral signatures associated with alteration zones, as they capitalize on specific absorption features of altered minerals. For instance, the (B4/B2) ratio was applied to the dataset to enhance the rock units containing iron oxides (refer to Figure 10). The distribution of iron oxides revealed through this approach demonstrates strong concordance with the existing lithological map.

Although the band ratio $(B6 \, / \, B7)$ is used to enhance the alteration of clay minerals, the band math of $[(B6 \, / \, B7) \, x \, (B4 \, / \, B5)]$ enhance the rocks with different alteration zones (Figure 11). The features from this map similar to the features from Figures $(8, \, 9, \, \text{and} \, 10)$. The band math of $[(B6 \, / \, B5) \, x \, (B4 \, / \, B5)]$ distinguish the felsic rocks from mafic rocks in Fig (12). The features from this map show similarities with the lithological map and the band combination maps. The mafic rocks are in dark colors and felsic rocks in bright colors.

The band ratio of (B6 / B2) shows the Fe bearing silicate rocks and distinguishes between the basement rocks and sedimentary rocks in Figure (13). The distribution of the units similar to the iron oxides rock units and to the basement rocks distribution in the area.

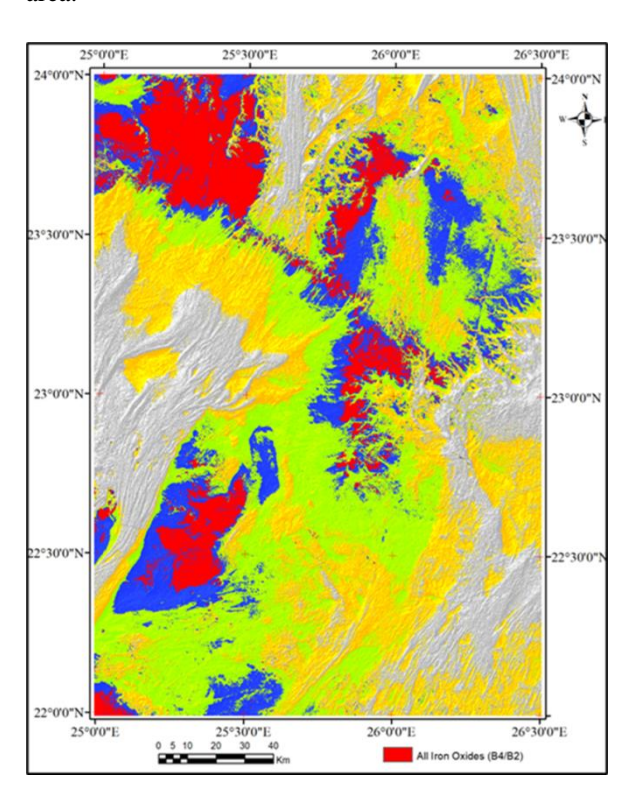


Fig. 10. The band ratio of (B4 / B2) enhance the rock unites contain iron oxides.

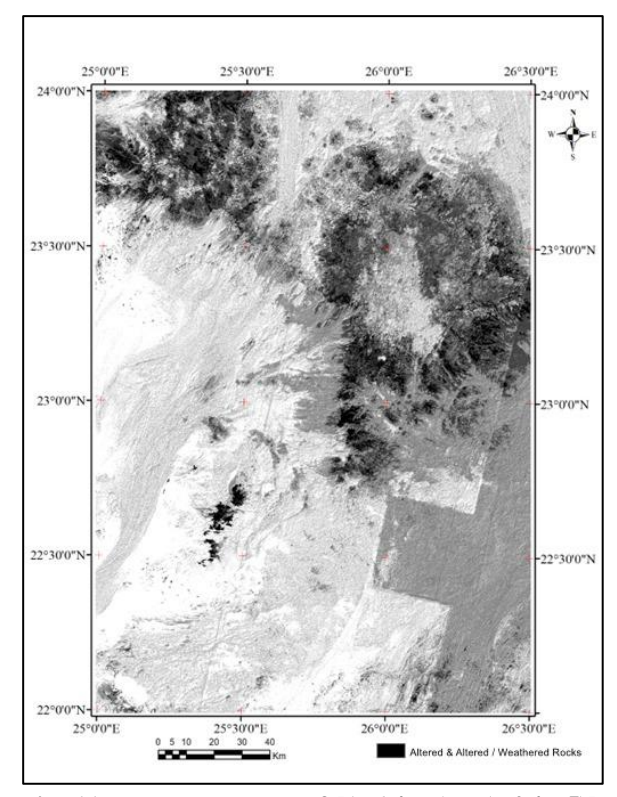


Fig. 11. The band math of [(B6 / B7) x (B4 / B5)] enhance the altered rock units in black.

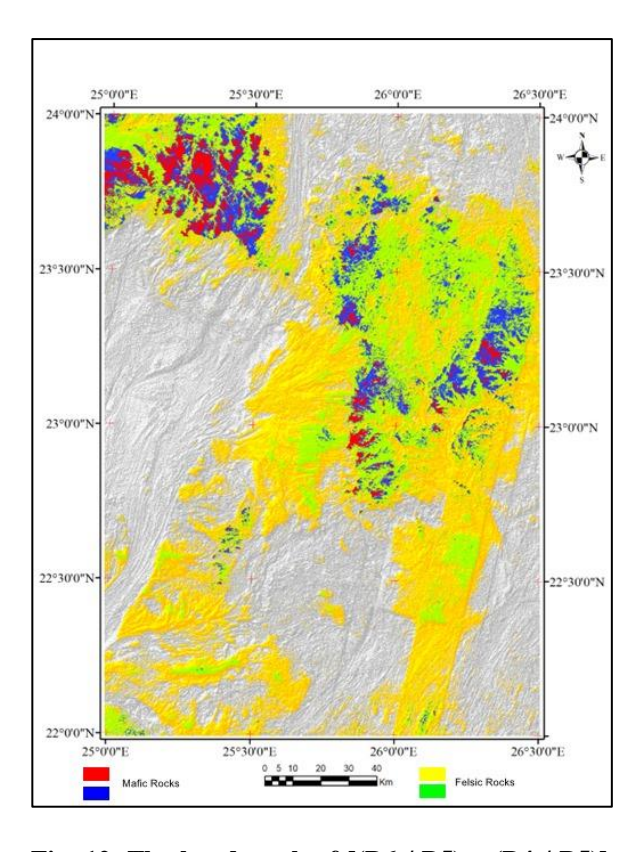


Fig. 12. The band math of $[(B6 / B5) \times (B4 / B5)]$ differentiates between the felsic and mafic rock units in the area.

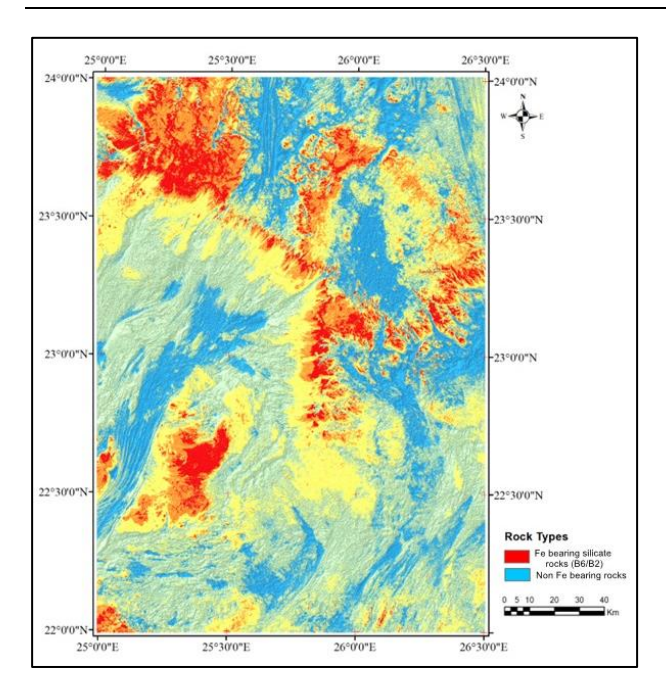


Fig. 13. The band ratio of $(B6\,/\,B2)$ shows the Fe bearing silicate units.

6. Conclusions

In an ideal situation, subsurface information from seismic data and well cores/logs are used to help constrain the interpreted basement structure and depth in gravity and magnetic structural models. In the East Uweinat/Gilf Kebir area, no such information exists. Consequently, the magnetic basement structure and depth estimates represent the only available subsurface "calibration points".

Magnetic anomalies maps show NE-SW/ENE-WSW banded distribution in positive and negative magnetic anomalies. These features are much obviously changed by some NW-SE trending faults possible cause of large-scale basement uplift (G. Uweinat).

Association of negative magnetic anomalies on the filtered maps indicates basinal areas or depo-centers intervening with the surrounding high basement blocks (could be major tilted fault blocks). Linear zones of magnetic gradients separating these uplifted and intervening basinal areas are ideal expression of dip-slip faults. The steepness of these zones of gradients is a direct measure to the dip angle of the faults.

The derivatives of the magnetic data provided much in improving the spatial and vertical resolution of the crystalline basement detailed structural fabric. The combination of the short-wavelength linear positive and negative anomalies is most probably the magnetic expression of the rift-parallel to sub-parallel horst and graben basement structures dominated in the area due to the rift – orthogonal NW-SE

extension. This is quite evident on the basement depth map.

Structurally, the area under study is mainly dominated by the major NE-SW trend. This NE-SW trend (oldest) is dissected and affected by a NW-SE trend (youngest). The E-W trend was assembled with the basin regions in the study area. The N-S trend is recognized in the area under investigation, especially in the region at the southern part of the area.

These structurally controlled basins are deep grabens with a thickness reached more than 3.5 km thick of young sedimentary infill, occupying the area between the major fault-blocks (basement blocks). Many intrabasin basement-cored horst structures were mapped. These represent promising exploration targets of potential hydrocarbon accumulations and for groundwater aquifers within those basins.

From the remote sensing data, there are some alteration processes that some of the rocks in the area have been exposed to, which are consistent with the geological map. In addition, the locations of Fesilicate mineralization are consistent with the basement rocks shown in the geological map.

By interpreting magnetic and satellite gravity data, it can be concluded that in the Gilf Kebir area, there are good conditions of hydrocarbon source-reservoir-cap assemblage. The deepest top of basement is about 3.5 km from sea level. The local structures are well developed.

7. Recommendations

As with any geological/geophysical study, this interpretation does not represent a final product but rather is something that can be extended, refined and modified as new data from gravity, seismic and/or wells become available for integration.

The interpretation should be updated and refined as more geological and geophysical data become available. We recommend that new constraints are integrated into the existing study as following:

- Acquiring and analysis of airborne gravity survey data.
- Acquiring seismic survey data

References

Abdelsalam, M.G., and Stern, R.J., (1996). Sutures and shear zones in the Arabian–Nubian Shield", *Journal of African Earth Sciences*, vol. 23, 289–310.

Abrams, M., and Hook, S.J., (1985). Simulated Aster data for geologic studies. J. IEEE Trans. Geosci. Remote Sens. 33 (3), 692-699.

Amer R., Kusky T. and El Mezayen A. (2012). Remote sensing detection of gold related alteration zones in Um Rus area, Central Eastern Desert of Egypt. Journal of Advances in Space Research, Elsevier, 49, 121-134.

Amuda, O.S., Adebisi, S., Jimoda, L., and Alade, A., (2014). Challenges and possible panacea to the municipal solid wastes management in Nigeria. J. Sust. Dev. Stud. 6 (1), 64-70.

Anderson, O. B., (2013). Marine gravity and Geoid from satellite altimetry, geoid determination – theory and

- *methods* (Chapter 9)", Ed. Fernando Sanso and Michael G. Sideris, Springer.
- Aydal, D., Ardal, E., and Dumanlilar, O., (2007).
 Application of the Crosta technique for alteration mapping of granitoidic rocks using ETM+ data: case study from eastern Tauride belt (SE Turkey). Int. J. Remote Sens. 28, 3895-3913.
- Blakely, R. J., and Simpson, R. W., (1986). "Approximating edges of source bodies from magnetic or gravity anomalies", *Geophysics*, vol. 51, no. 7, 1494-1498
- Conoco Coral and EGPC, (1987). Geological map of Egypt, Geologic map of Owinat El Gilf El Kebir, Scale 1: 500,000", *Geological survey of Egypt (EGS)*.
- Cordell, Lindrith, and Grauch, V.J.S., (1985). Mapping basement magnetization zones from aeromagnetic data in the San Juan basin, New Mexico in the utility of regional gravity and magnetic anomaly maps", Hinze, W.J., ed., Society of Exploration Geophysicists, 181-197.
- Dixon, T.H., and Golombek, M.P., (1988). Late Precambrian crustal accretion rates in northeast Africa and Arabia", *Geology*, vol. 16, 991–994.
- Gaber S., Ghulam A. and Kusky T. (2010). Detecting areas of high-potential gold mineralization using ASTER data. Journal of Ore Geology Reviews, Elsevier, 38, 59-69.
- Gibson, G.M., Morse, M.P., Ireland, T.R., and Nayak, G.K., (2011). Arc-continent collision and orogenesis in western Tasmanides: insights from reactivated basement structures and formation of an oceancontinent transform boundary off western Tasmania", Gondwana Res., vol. 19, 608-627.
- Goetz, A.F.H., Rock, B.N., and Rowan, L.C., (1983).Remote sensing for exploration: an overview. Econ. Geol. 78, 573-590.
- Hall, L., Hackney, R., and Johnston, S., (2012). "Understanding Australia's southwest margin: basement architecture as a framework for predictive basin analysis", Aus Geo News, 105.
- Harris, N.B.W., Hawkesworth, C., and Tindle, A.G., (1993). The growth of continental crust during the late Proterozoic: geochemical evidence from the Arabian shield, in Magmatic Processes and Plate Tectonics", Geological Society Special Publication, Prichard, H.M., Alabaster, T., Harris, N.B.W., Neary, C.R. (Eds.), pp. 363–371
- Ishagh M.M., Pour A.B., Benali H., Idriss A.M., Reyoug S.A.S., Muslim A.M., and Hossain M.S. (2021) Lithological and alteration mapping using Landsat 8 and ASTER satellite data in the Reguibat Shield (West African Craton), North of Mauritania: implications for uranium exploration. Arab Journal of Geosciences, 14, p. 2576
- Kroner, A., Greiling, R.O., Reischmann, T., Hussain, I.M., Stern, R.J., Durr, St., Kruger, J., and Zimmer, M., (1987) Pan-African crustal evolution in northeast Africa, in *Proterozoic Lithospheric Evolution*, Geodynamic Series", Kroner, A. (Ed.), American Geophysical Union, vol. 17. pp. 235–257.
- Li, C.-F., Zhou, Z., Li, J., Chen, B., and Geng, J., (2008) Magnetic zoning and seismic structure of the South China Sea Ocean basin", *Mar. Geophys. Res.*, vol. 29, 223-238.
- Li, X., 2006: "Understanding 3D analytic signal amplitude", *Geophysics*, vol. 71, L13-L16.

- Liu, J.P., Song, M., Horton, R.M., and Hu, Y., (2013). Reducing spread in climate model projections of a September ice-free Arctic. Proc. Natl. Acad. Sci. 110, 12571-12576.
 - http://dx.doi.org/10.1073/pnas.1219716110.
- MacLeod, I. N., Jones, K. and Dai, T. F., (1993). 3-D Analytic signal in the interpretation of total magnetic field data at low magnetic latitudes", *Exploration Geophysics*, vol. 24, 679-688.
- Meshref, W. M., 1990: "Tectonic framework, in *Geology of Egypt* (Chapter VII)", Ed. R. Said, Balkema, Rotterdam, Book field.
- Mia, M.B., and Fujimitsu, Y., (2012) Mapping hydrothermal altered mineral deposits using Landsat 7 ETM+ image in and around Kuju volcano, Kyushu, Japan. J. Earth Syst. Sci. 121 (4), 1049-1057.
- Morse, M., (2010) Potential field methods prove effective for continental margin studies", AusGeo News, 98.
- Nuclear Materials Authority (NMA), 2011: "Highresolution airborne magnetic survey over El Gelf El Kebir area, southwest western desert, Egypt", Internal report on behalf of Ganoub El-Wadi Holding Petroleum Company (Ganope).
- Okada, K., Segawa, K., and Hayashi, I., 1993: Removal of the vegetation effect from LANDSAT TM and GER imaging spectroradiometer data. ISPRS J. Photogrammet. Remote Sens. 48 (6), 16-27.
- Oldenburg, D. W., (1974) "The inversion and interpretation of gravity anomalies", *Geophysics*, vol. 39, 424–438.
- Poormirzaee, R., and Oskouei, M.M., (2010) Use of spectral analysis for detection of al-terations in ETM data, Yazd, Iran. Appl. Geomatica 2 (4), 147-154.
- Pour A.B. and Hashim, M. (2011): Identification of Hydrothermal Alteration Minerals for Exploring of Porphyry Copper Deposit Using ASTER Data SE Iran. Journal of Asian Earth Sciences, Elsevier, 42, 1309-1323.
- Pour A.B., Hashim M., Hong J.K. and Park Y. (2019): Lithological and alteration mineral mapping in poorly exposed lithologies using Landsat-8 and ASTER satellite data: North-eastern Graham Land, Antarctic Peninsula. Journal of Ore Geology Reviews, Elsevier, 108, 112-133.
- Ramadan, T.M., Abdelsalam, M.G., and Stern, R.J., 2001: Mapping gold-bearing massive sulfide deposits in the neoproterozoic Allaqi Suture, Southeast Egypt with Landsat TM and SIR-C/X SAR images. Photogrammet. Eng. Remote Sens. 67 (4), 491-497.
- Ramsay, J.G., and Huber, M.I., 1987: "The techniques of modern structural geology. In: Folds and Fractures, vol.
 2. Academic Press, London, Orlando, San Diego, New York, Austin, Boston, Sydney, Tokyo, Toronto xi + 391 pp.
- Ren, D., and Abdelsalam, M.G., 2006: "Tracing along-strike structural continuity in the Neoproterozoic Allaqi-Heiani Suture, southern Egypt using principal component analysis (PCA), fast Fourier transform (FFT), and redundant wavelet transform (RWT) of ASTER data", Journal of African Earth Sciences, vol. 44, 181–195.
- Roest, W. R., Verhoef, J. and Pilkington, M., 1992: "Magnetic interpretation using 3-D analytic signal", *Geophysics*, vol. 57, 116-125.
- Rowan, L.C., Kingstone, M.J., and Crowley, J.K., 1986: Spectral reflectance of carbonatite and related alkalic igneous rocks for four North American localities. Econ. Geol. 81, 857-871.

- Sabin's, F.F., 1997: Remote Sensing; Principals and Interpretation, fourth ed. Freeman, San Francisco, p. 449.
- Sabin's, F.F., 1999: Remote sensing for mineral exploration. Ore Geol. Rev. 14, 157-183.
- Salem, A., Williams, S., Fairhead, J.D., Smith, R., and Ravat, D., 2008: "Interpretation of magnetic data using tilt-angle derivatives", *Geophysics*, vol. 73, no. 1, L1-L10.
- Sekandari, M., Masoumi, I., Pour, A.B., Muslim, A.M., Rahmani, O., Hashim, M., Zoheir, B., Pradhan, B., Misra, A., and Aminpour, S.M., (2020) Application of Landsat-8, Sentinel-2, ASTER and WorldView-3 Spectral Imagery for Exploration of Carbonate-Hosted Pb-Zn Deposits in the Central Iranian Terrane (CIT). Remote Sensing, 12, 1239.
- Spector, A., (1968) Spectral analysis of aeromagnetic maps", Ph. D. Thesis, Department of physics, *Univ. of Toronto*, Canada.

- Stein, M., and Goldstein, S.L., (1996). From plume head to continental lithosphere in the Arabian–Nubian Shield", *Nature*, vol. 382, 773–778.
- Stern, R.J., (1994) "Arc assembly and continental collision in the Neoproterozoic East African Orogen: Implications for the consideration of Gondwanaland", Annual Review of Earth and Planetary Sciences, vol. 22, 319–351.
- Tangestani, M.H., and Moore, F., (2000). Iron oxide and hydroxyl enhancement using the Crosta method: a case study from the Zagros belt, Fars Province, Iran. Int. J. Appl. Earth Observ. Geoinform. 2 (2), 140-146.
- Vervoort, J.D., and Blichert-Toft, J., (1999). "Evolution of the depleted mantle: Hf isotope evidence from juvenile rocks through time", *Geochimica et Cosmochimica Acta*, vol. 63, 533–556.